

Description and validation of a flexible fiber model, implemented in a general-purpose CFD code

Jelena Andric^[1], Stefan B. Lindström^[2], Srdjan Sasic^[1] and Håkan Nilsson^[1]

¹ Department of Applied Mechanics, Chalmers University of Technology, 412 96 Göteborg, Sweden

² Department of Management and Engineering, The Institute of Technology, Linköping University, 581 83 Linköping, Sweden

Keywords: flexible fiber model, particle level simulation, open-source CFD

Abstract

A flexible fiber model has been implemented in a general-purpose, open-source computational fluid dynamics code. The fibers are modeled as chains of cylindrical segments. Each segment is tracked individually and their equations of motion account for the hydrodynamic forces and torques from the interaction with the fluid, the elastic bending and twisting torques, and the connectivity forces and moments that ensure the fiber integrity. The segment inertia is taken into account and a one-way coupling with the fluid phase is considered. The model is applied to the rotational motion of an isolated fiber in a low segment Reynolds number shear flow. In the case of a stiff, straight fiber, the computed period of rotation is in good agreement with the one computed using Jeffery's equation for an equivalent spheroid aspect ratio. A qualitative comparison is made with experimental data for flexible fibers. These results show that the implemented model can reproduce the known dynamics of rigid and flexible fibers successfully.

Introduction

The dynamics of particles suspended in flowing fluid are of great interest and importance in many industrial processes. Particularly, suspensions of fibers and fiber flocs are processed to produce paper products and fiber composites. One example is the making of pulp mats for use in hygiene products. When a fiber suspension is made to flow, the fibers translate, rotate and deform into configurations that become locked into the formed product. These changes in the microstructures of the suspension affect the macroscopic properties of the produced material, such as elastic modulus, strength, and thermal and electric conductivities. In pulp and paper processing, the fiber dynamics of the sheet forming process are one of the most important factors that influence the sheet characteristics (Ross and Klingenberg 1997; Matsuoka and Yamamoto 1995).

To model these industrial processes, including wet forming of paper and dry forming of pulp mats, it is necessary to consider large particle systems in high Reynolds number flow with finite Reynolds number fiber–flow interactions (Lindström 2008). The forming unit process in water-based papermaking has been previously modeled at a particle-level with direct numerical simulation (DNS) under a Stokes flow assumption (Svenning et al. 2012) and with a microhydrodynamics approach for finite Reynolds numbers (Lindström and Uesaka 2008; Lindström et al. 2009). The characteristics of dry forming, with large flow geometries and fibers suspended in air, present a numerically even more challenging conditions, since air is less dissipative than water.

This work constitutes a first step toward a complete model for air-fiber suspensions modeling, and thus considers the motion of isolated fibers in shear flow.

There has been experimental work on the behavior of fibers in different flow conditions. Forgacs and Mason (1959a,b) identified different regimes for fiber motion in creeping shear flow. They observed that flexible fibers move in different regimes of motion, stiff, spring-like and a coiled regime with or without entanglement, depending on the fiber stiffness, length, and the flow properties such as shear rate and fluid viscosity.

A number of numerical approaches have been developed to study particle-laden flows. In the Eulerian–Eulerian approach the phases are treated as interpenetrating continua. The Lagrangian–Eulerian approach, on the other hand, treats particles as moving objects in a fluid medium. In the DNS approach, the particle geometries are resolved to a high level of detail, giving excellent predictive capability for fiber motion in suspension (Qi 2006; Salahuddin et al. 2012), but at a relatively high computational cost. In the microhydrodynamics approach, many particles are combined into a multi-rigid-body system. The choice of model is always a trade-off between accuracy and system size, as previously discussed by Crowe et al. (1998), Lindström and Uesaka (2007) and Hämäläinen et al. (2011).

Several variants of the microhydrodynamics approach have been previously developed to simulate flexible fiber motion in shear and sedimentation flows. Matsuoka and Yamamoto (1995) developed a particle-level simulation technique to capture the dynamics of rigid and flexible fibers in a prescribed flow field. They represented a fiber by a set of spheres, lined up and connected to each

neighboring sphere. Ross and Klingenberg (1997) proposed a similar model, but using a chain of rigid, prolate spheroids. These numerical studies were in qualitative agreement with the experimental results of isolated fiber motion obtained by Forgacs and Mason (1959a,b) and also predicted some of the rheological properties of fiber suspensions. Schmid et al. (2000) developed a particle-level simulation technique to study flocculation of fibers in sheared suspensions in three dimensions. They investigated the influence of the shear rate, fiber shape, fiber flexibility, and frictional inter-particle forces on flocculation. The fibers were modeled as chains of massless, rigid cylinder segments interacting with an imposed flow field through viscous drag forces and with other fibers through contact forces. Lindström and Uesaka (2007) further developed the model of Schmid et al. (2000), by taking into account the particle inertia and the intermediate to long-range hydrodynamic interactions between the fibers. They derived an approximation for the non-creeping interaction between the fiber segments and the surrounding fluid, for finite segment Reynolds numbers, and took into account the two-way coupling between the particles and the carrying fluid. Their simulations successfully reproduced the different regimes of motion for threadlike particles (Lindström and Uesaka 2007), and were subsequently used to study paper forming (Lindström and Uesaka 2008; Lindström et al. 2009).

In the present work, a model similar to the flexible fiber model developed by Lindström and Uesaka (2007) is implemented in the OpenFOAM, open source computational fluid dynamics (CFD) software (Weller et al. 1998). The model is applied to simulate the motion of an isolated cylindrical flexible fiber in a low segment Reynolds number simple shear flow. The simulation results are compared with experimental and analytical results available in the literature.

Nomenclature

Roman symbols

d	diameter (m)
l	length (m)
m	mass (kg)
r	position (m)
$\dot{\vec{r}}$	velocity (ms ⁻¹)
$\ddot{\vec{r}}$	acceleration (ms ⁻²)
\hat{z}	orientation vector (-)
\overline{I}	inertia tensor (kgm ²)
$\dot{\overline{I}}$	inertia tensor time derivative (kgm ² s ⁻¹)
\vec{F}	force (N)
\vec{X}	connectivity force (N)
\vec{T}	torque (Nm)
\vec{Y}	bending and twisting torque (Nm)
\overline{A}	resistance tensor (kgs ⁻¹)
\overline{C}	resistance tensor (kgs ⁻¹)
\overline{H}	resistance tensor (kgs ⁻¹)

C_D	drag coefficient (-)
Re	Reynolds number (-)
T	oscillatory period (s)
Δt	time step (s)

Greek symbols

ρ	density (kgm ⁻³)
η	dynamic viscosity(kgm ⁻¹ s ⁻¹)
$\dot{\gamma}$	shear rate (s ⁻¹)
$\overline{\delta}$	Kronecker delta symbol (-)
$\vec{\omega}$	angular velocity (s ⁻¹)
\vec{v}	fluid velocity (ms ⁻¹)
$\vec{\Omega}$	fluid angular velocity (s ⁻¹)
\overline{E}	strain rate tensor (s ⁻¹)

Subscripts

i	segment index
n	time step index
s	segment

Superscripts

h	hydrodynamic
v	viscous
I	dynamic
ω	body
b	bending
t	twisting

Fiber Model

First the fiber geometry and the governing equations for fiber motion are described. The hydrodynamic forces and torques, and bending and twisting torques are then presented. The numerical algorithms to solve the discretized governing equations and the constraints on the discretization time step are also discussed.

Fiber Geometry. A fiber is modeled as a chain of N rigid cylindrical segments (Schmid et al. 2000; Lindström and Uesaka 2007), see Fig. 1. The segments are indexed $i \in 1, N$ and their locations are specified with respect to a global Cartesian coordinate system Γ . The axes of this inertial frame are defined by the base vectors $\{\hat{e}_1, \hat{e}_2, \hat{e}_3\}$ and the origin is denoted by O . A single fiber segment has a diameter d_i , a length l_i , a start point P_i , and a unit vector \hat{z}_i , which is aligned with the segment. The position of each fiber segment's center of mass is thus $\vec{r}_i = \vec{OP}_i + l_i \hat{z}_i / 2$.

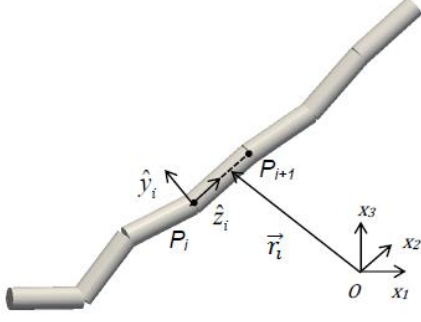


Figure 1: Fiber geometry definitions

The fiber equilibrium shape needs to be included in the geometry description. For this purpose, a local coordinate system Γ_i is defined for each segment. Γ_i is a right-hand orthogonal coordinate system with axes $\{\hat{x}_i, \hat{y}_i, \hat{z}_i\}$ and origin P_i . The fiber equilibrium shape is then defined by fixing a local coordinate system $\{\hat{x}_i, \hat{y}_i, \hat{z}_i\}$ on each segment i and an equilibrium coordinate system $\{\hat{x}_i^{eq}, \hat{y}_i^{eq}, \hat{z}_i^{eq}\}$ for each segment i on its preceding segment $i-1$. For a given local coordinate system Γ_{i-1} for segment $i-1$, the angles ϕ_i and θ_i of twist and bend respectively can be determined, so that coordinate system Γ_i^{eq} can be calculated from Γ_{i-1} . First, Γ_{i-1} is rotated an angle ϕ_i about \hat{z}_i , which gives Γ_i^1 with coordinate axes $\{\hat{x}_i^1, \hat{y}_i^1, \hat{z}_i^1\}$. Γ_i^1 is then rotated an angle θ_i about \hat{y}_i^1 and Γ_i^{eq} is obtained.

Equations of Motion. The equations of motion comprise Euler's first and second law for each fiber segment i , as formulated by Schmid et al. 2000; Lindström and Uesaka 2007, yielding

$$m_i \ddot{\vec{r}}_i = \vec{F}_i^h + \vec{X}_{i+1} - \vec{X}_i \quad (1)$$

$$\frac{\partial(\vec{I}_i \cdot \vec{\omega}_i)}{\partial t} = \vec{T}_i^h + \vec{Y}_{i+1} - \vec{Y}_i + \frac{l_i}{2} \hat{z}_i \times \vec{X}_{i+1} + \left(\frac{-l_i}{2} \hat{z}_i \right) \times (-\vec{X}_i) \quad (2)$$

In Eq. (1), m_i is the mass of the segment i , \vec{F}_i^h is the hydrodynamic force acting on the segment i and \vec{X}_i is the connectivity force exerted on segment $i-1$ by segment i . For the end segments $\vec{X}_1 = \vec{X}_{N+1} = 0$. In Eq. (2), \vec{I}_i is the tensor of inertia of segment i with respect to Γ , $\vec{\omega}_i$ is the angular velocity, \vec{T}_i^h is the hydrodynamic

torque and \vec{Y}_i is the sum of the bending and twisting torques exerted on segment $i-1$ by segment i . For the end segments $\vec{Y}_1 = \vec{Y}_{N+1} = 0$. It is required that the end-points of adjacent fiber segments coincide, *i.e.*

$$\vec{r}_i + \frac{l_i}{2} \hat{z}_i = \vec{r}_{i+1} - \frac{l_{i+1}}{2} \hat{z}_{i+1}. \quad (3)$$

A connectivity equation is then obtained by taking the time derivative of Eq. (3), yielding

$$\dot{\vec{r}}_i - \dot{\vec{r}}_{i+1} = \frac{l_i}{2} \vec{\omega}_i \times \hat{z}_i + \frac{l_{i+1}}{2} \vec{\omega}_{i+1} \times \hat{z}_{i+1}. \quad (4)$$

Hydrodynamic Forces. First, we define the segment Reynolds number as $Re_s = \rho \Delta v / \eta$, where ρ is the density of the fluid, η is its dynamic viscosity, d is the fiber diameter and Δv is the characteristic velocity difference between the fibers and the fluid. Here, we choose $\Delta v = l \dot{\gamma}$, where $\dot{\gamma}$ is the characteristic shear rate of the flow. The hydrodynamic forces are dominated by viscous effects at small segment Reynolds numbers $Re_s \ll 1$, and by inertia effects for large segment Reynolds numbers $Re_s \gg 1$. Lindström and Uesaka (2007) numerically investigated the consequence of expressing viscous and inertia drag as a sum of two separable components, and found a fair agreement between the model, theory and experiments for a cylinder in cross-flow in the viscous flow regime, $Re_s \leq 10^{-1}$, as well as in the regime dominated by dynamic effects, $10^2 \leq Re_s \leq 3 \times 10^5$. The maximum error in drag coefficient C_D is 42%, found in the intermediate interval of Reynolds numbers at $Re_s \approx 5.4$ (Re_s was based on the cross-flow velocity in those numerical experiments). The total force and torque exerted on fiber segment i by the fluid are then given by

$$\vec{F}_i^h = \vec{F}_i^{h,v} + \vec{F}_i^{h,I} \quad (5)$$

$$\vec{T}_i^h = \vec{T}_i^{h,v} + \vec{T}_i^{h,I} \quad (6)$$

The viscous drag force of a fiber segment is here approximated with that of a prolate spheroid. An analytical solution described by Kim and Karilla (1991) is available for the viscous drag force on an isolated spheroidal particle under laminar conditions. According to the semi-empirical formula of Cox (1971), a prolate spheroid is hydrodynamically equivalent to a finite circular cylinder in the sense that their orbiting behavior in shear flow is the same if

$$\frac{r_e}{r_c} = 1.24 (\ln r_c)^{-1/2}, \quad (7)$$

where r_e is the equivalent aspect ratio of the prolate spheroid and r_c is the cylinder aspect ratio. For fiber segment i with aspect ratio $r_c = l_i/d_i$, We choose the major axis of the hydrodynamically equivalent prolate spheroid to be $a_i = l_i$. Its minor axis, b_i is then obtained by inserting $r_e = a_i/b_i$ into Cox's formula as

$$b_i = \frac{1}{1.24} d_i \sqrt{\ln \frac{l_i}{d_i}}. \quad (8)$$

Cox's formula is valid for isolated particles and a slender-body approximation. None of these assumptions are true for fiber segments. However, Lindström and Uesaka (2007) performed numerical experiments, which have shown that the error in the model predictions of orbit period of rigid fibers in shear flow is less than 3.4% compared to Eq. (7) for $r_c \geq 10$ when a two-way coupling is considered. Thus, for a given velocity field \vec{v} of the fluid, the viscous hydrodynamic force $\vec{F}_i^{h,v}$ and torque $\vec{T}_i^{h,v}$ are defined by

$$\vec{F}_i^{h,v} = \bar{\bar{A}}_i^v \cdot (\vec{v}(\vec{r}_i) - \dot{\vec{r}}_i) \quad (9)$$

$$\vec{T}_i^{h,v} = \bar{\bar{C}}_i^v \cdot (\vec{\Omega}(\vec{r}_i) - \dot{\vec{\omega}}_i) + \bar{\bar{H}}_i^v : \bar{\bar{E}}(\vec{r}_i). \quad (10)$$

Here, $\vec{\Omega} = \nabla \times \vec{v}/2$ is the angular velocity of the fluid and $\bar{\bar{E}} = \nabla \vec{v} + (\nabla \vec{v})^T/2$ is the strain rate tensor, with \mathbf{T} the transpose. The operators ∇ and $\nabla \times$ denote the gradient and the curl, respectively. The hydrodynamic resistance tensors $\bar{\bar{A}}_i^v$, $\bar{\bar{C}}_i^v$ and $\bar{\bar{H}}_i^v$ are defined as

$$\bar{\bar{A}}_i^v = 3\pi\eta l_i (Y_i^A \bar{\delta} + (X_i^A - Y_i^A) \hat{z}_i \hat{z}_i) \quad (11)$$

$$\bar{\bar{C}}_i^v = \pi\eta l_i^3 (Y_i^C \bar{\delta} + (X_i^C - Y_i^C) \hat{z}_i \hat{z}_i) \quad (12)$$

$$\bar{\bar{H}}_i^v = -\pi\eta l_i^3 Y_i^H (\bar{\bar{\epsilon}} \cdot \hat{z}_i) \hat{z}_i, \quad (13)$$

where $\bar{\delta}$ and $\bar{\bar{\epsilon}}$ are the unit and the permutation tensor, respectively. The hydrodynamic coefficients X_i^A , Y_i^A , X_i^C , Y_i^C and Y_i^H depend on the eccentricity $e_i = (1 - b_i^2/a_i^2)^{1/2}$ and are according to Kim and Karilla (1991) defined as

$$L(e_i) = \ln \frac{1+e_i}{1-e_i}$$

$$X_i^A(e_i) = \frac{8}{3} e_i^3 (-2e_i + (1+e_i^2)L(e_i))^{-1}$$

$$Y_i^A(e_i) = \frac{16}{3} e_i^3 (2e_i + (3e_i^2 - 1)L(e_i))^{-1}$$

$$X_i^C(e_i) = \frac{4}{3} e_i^3 (1-e_i^2)(2e_i - (1-e_i^2)L(e_i))^{-1} \quad (14)$$

$$Y_i^C(e_i) = \frac{4}{3} e_i^3 (2-e_i^2)(-2e_i - (1+e_i^2)L(e_i))^{-1}$$

$$Y_i^H(e_i) = \frac{4}{3} e_i^5 (-2e_i + (1+e_i^2)L(e_i))^{-1}.$$

In the range $10^2 \leq Re_s \leq 3 \times 10^5$ of segment Reynolds numbers, the inertia drag force of a cylinder in cross-flow is dominant as compared to the viscous drag in the axial or cross-direction. If \hat{z}_i is the cylinder orientation, then only the flow components in the plane perpendicular to \hat{z}_i need to be considered. The drag coefficient for cross flow over a circular cylinder is, according to Tritton (1988), $C_D^I = 1$, for $10^2 \leq Re_s \leq 3 \times 10^5$. The total drag force and torque on a cylindrical fiber segment are obtained through integration over the infinitesimal cylinder slices. The dynamic drag force and torque are then given by

$$\vec{F}_i^{h,I} \approx \bar{\bar{A}}_i^I \cdot (\vec{v}(\vec{r}_i) - \dot{\vec{r}}_i) \quad (15)$$

$$\vec{T}_i^{h,I} \approx \bar{\bar{C}}_i^I \cdot (\vec{\Omega}(\vec{r}_i) - \dot{\vec{\omega}}_i) + \bar{\bar{H}}_i^I : \bar{\bar{E}}(\vec{r}_i), \quad (16)$$

where the dynamic drag resistance tensors are

$$\bar{\bar{A}}_i^I = \frac{1}{2} C_D^I \rho d_i l_i \nu_{\perp,i} (\bar{\delta} - \hat{z}_i \hat{z}_i) \quad (17)$$

$$\bar{\bar{C}}_i^I = \frac{1}{24} C_D^I \rho d_i l_i^3 \nu_{\perp,i} (\bar{\delta} - \hat{z}_i \hat{z}_i) \quad (18)$$

$$\bar{\bar{H}}_i^I = \frac{1}{24} C_D^I \rho d_i l_i^3 \nu_{\perp,i} (\bar{\bar{\epsilon}} \cdot \hat{z}_i) \hat{z}_i \quad (19)$$

and $\nu_{\perp,i} = |(\bar{\delta} - \hat{z}_i \hat{z}_i) \cdot (\vec{v}(\vec{r}_i) - \dot{\vec{r}}_i)|$ is the cross-flow velocity of the fluid relative to the fiber segment.

Bending and twisting torques. The bending and twisting torque exerted by segment $i-1$ on segment i are denoted by \vec{Y}_i^b and \vec{Y}_i^t , respectively, and taken into account in Eq. (2) as $\vec{Y}_i = \vec{Y}_i^b + \vec{Y}_i^t$. Bending and twisting torques act to restore the fiber shape when it is deformed out of its equilibrium. The bending torque exerted by segment $i-1$ on segment i is

$$\vec{Y}_i^b = -k_{b,i} \alpha_{b,i} \hat{e}_{b,i}. \quad (20)$$

Here, $k_{b,i}$ is a bending constant, $\alpha_{b,i} = \arccos(\hat{z}_i \cdot \hat{z}_i^{eq})$ is the bending angle, and

$\hat{e}_{b,i} = (\hat{z}_i \times \hat{z}_i^{eq}) / |\hat{z}_i \times \hat{z}_i^{eq}|$ is the bending torque direction. The bending constant $k_{b,i}$ is related to the bending stiffness of an elastic cylinder as $k_b = E_Y(I_{i-1} + I_i)/(l_{i-1} + l_i)$, where E_Y is the Young's modulus of the fiber material, and $I_i = \pi d_i^4/64$ is the area moment of inertia of a circular cylinder with diameter d_i . The twisting torque exerted by segment $i-1$ on segment i is

$$\vec{Y}_i^t = -k_{t,i} \alpha_{t,i} \hat{c}_i. \quad (21)$$

Here $k_{t,i}$ is the twisting constant,

$$\alpha_{t,i} = \arccos(\hat{y}_i^\perp \cdot \hat{y}_i^{eq,\perp}) \text{ is the twisting angle, and}$$

$$y_i^\perp = \frac{(\bar{\delta} - \hat{c}_i \hat{c}_i) \cdot \hat{y}_i}{|(\bar{\delta} - \hat{c}_i \hat{c}_i) \cdot \hat{y}_i|}, \quad y_i^{eq,\perp} = \frac{(\bar{\delta} - \hat{c}_i \hat{c}_i) \cdot \hat{y}_i^{eq}}{|(\bar{\delta} - \hat{c}_i \hat{c}_i) \cdot \hat{y}_i^{eq}|},$$

where $\hat{c}_i = (\vec{r}_i - \vec{r}_{i-1}) / |\vec{r}_i - \vec{r}_{i-1}|$. The twisting constant $k_t = G(J_{i-1} + J_i)/(l_{i-1} + l_i)$, where G is the shear modulus of the material and $J_i = \pi d_i^4/32$ is the corresponding area moment of inertia.

Discretized Fiber Equations of Motion. The fiber equations of motion are discretized in time with a time step Δt . Subscripts $n-1$ and n denote the previous and the current time step, respectively. An implicit numerical scheme is used for calculating the segment velocity and angular velocity to enhance numerical stability. In all the equations presented in this section, the connectivity forces \vec{X}_i and \vec{X}_{i+1} are treated as unknowns. Using the expression for the hydrodynamic force, Eq. (1) can be discretized as

$$\frac{m}{\Delta t} (\dot{\vec{r}}_{i,n} - \dot{\vec{r}}_{i,n-1}) = (\bar{A}_{i,n-1}^v + \bar{A}_{i,n-1}^I) \cdot \dot{\vec{r}}_{i,n-1} + (\bar{v}(\vec{r}_{i,n-1}) - \dot{\vec{r}}_{i,n-1}) + \vec{X}_{i+1,n} - \vec{X}_{i,n}. \quad (22)$$

In the angular momentum equation (2), the time differential term can be discretized as

$$\frac{\partial(\bar{I}_{i,n-1} \cdot \bar{\omega}_{i,n})}{\partial t} = \dot{\bar{I}}_{i,n-1} \cdot \bar{\omega}_{i,n} + \bar{I}_{i,n-1} \cdot \dot{\bar{\omega}}_{i,n}$$

$$\approx \dot{\bar{I}}_{i,n-1} \cdot \bar{\omega}_{i,n} + \frac{1}{\Delta t} \bar{I}_{i,n-1} \cdot (\bar{\omega}_{i,n} - \bar{\omega}_{i,n-1}). \quad (23)$$

Using the expression for the hydrodynamic force, Eq. (2) yields

$$\dot{\bar{I}}_{i,n-1} \cdot \bar{\omega}_{i,n} + \frac{1}{\Delta t} \bar{I}_{i,n-1} \cdot (\bar{\omega}_{i,n} - \bar{\omega}_{i,n-1}) =$$

$$(\bar{C}_{i,n-1}^v + \bar{C}_{i,n-1}^I) \cdot (\bar{\Omega}(\vec{r}_{i,n-1}) - \bar{\omega}_{i,n}) +$$

$$(\bar{H}_{i,n-1}^v + \bar{H}_{i,n-1}^I) : \bar{E}(\vec{r}_{i,n-1}) + \vec{Y}_{i+1,n-1} -$$

$$\vec{Y}_{i,n-1} + \frac{l_i}{2} \hat{z}_{i,n-1} \times (\vec{X}_{i+1,n} + \vec{X}_{i,n}). \quad (24)$$

Finally, Eq. (4) is discretized as

$$\dot{\vec{r}}_{i,n} - \dot{\vec{r}}_{i+1,n} = \frac{l_i}{2} \bar{\omega}_{i,n} \times \hat{z}_{i,n-1} + \frac{l_{i+1}}{2} \bar{\omega}_{i+1,n} \times \hat{z}_{i+1,n-1}.$$

.....(25)

The momentum equation (22), the angular momentum equation (24) and the connectivity equation (25) form a system of equations, which can be solved for the unknown connectivity forces, velocities and angular velocities at time n . Since these variables have different physical units, the coefficients of the linear system will differ by many orders of magnitude and make the system ill-conditioned. Thus, a system of dimensionless equations should be considered.

Dimensionless Connectivity Force Linear System.

The dimensionless system of equations for the unknown connectivity forces, where (*) denotes dimensionless quantities, reads

$$\bar{Q}_i^* \cdot \bar{X}_{i,n}^* + \bar{S}_i^* \cdot \bar{X}_{i+1,n}^* + \bar{T}_i^* \cdot \bar{X}_{i+2,n}^* = \bar{V}_i^*. \quad (26)$$

The corresponding dimensionless tensors are known for the previous time step and the subscript $n-1$ is omitted for convenience. These tensors read

$$\bar{Q}_i^* = -\left(\frac{m^*}{\Delta t^*} \bar{\delta} + \bar{A}_i^{v*} + \bar{A}_i^{I*}\right)^{-1} + \frac{3}{4r_p} \bar{C}_{z\ i}^*$$

$$\bar{S}_{i,n-1}^* = \left(\frac{m^*}{\Delta t^*} \bar{\delta} + \bar{A}_i^{v*} + \bar{A}_i^{I*}\right)^{-1} +$$

$$\left(\frac{m^*}{\Delta t^*} \bar{\delta} + \bar{A}_{i+1}^{v*} + \bar{A}_{i+1}^{I*}\right)^{-1}$$

$$+ \frac{3}{4r_p} \bar{C}_{z\ i}^* + \frac{3}{4r_p} \bar{C}_{z\ i+1}^*$$

$$\bar{T}_{i,n-1}^* = -\left(\frac{m^*}{\Delta t^*} \bar{\delta} + \bar{A}_{i+1}^{v*} + \bar{A}_{i+1}^{I*}\right)^{-1} + \frac{3}{4r_p} \bar{C}_{z\ i+1}^*$$

$$\bar{V}_i^* = -(\bar{s}_i^* - \bar{s}_{i+1}^* + r_p(\bar{b}_i^* + \bar{b}_{i+1}^*))$$

$$\bar{s}_i^* = \left(\frac{m^*}{\Delta t^*} \bar{\delta} + \bar{A}_i^{v*} + \bar{A}_i^{I*}\right)^{-1} \cdot \left(\frac{m^*}{\Delta t^*} \dot{\vec{r}}_i^* +$$

$$+ (\bar{A}_i^{v*} + \bar{A}_i^{I*}) \cdot \bar{v}^*(\vec{r}_i)\right)$$

$$\bar{b}_i^* = \left(\left(\bar{I}_i^* + \frac{1}{\Delta t^*} \bar{I}_i^* + \bar{C}_i^{v*} + \bar{C}_i^{I*}\right)^{-1} \cdot \left(\frac{1}{\Delta t^*} \bar{I}_i^* \cdot \bar{\omega}_i^* +$$

$$(\bar{C}_i^{v*} + \bar{C}_i^{I*}) \cdot \bar{\Omega}^*(\vec{r}_i) + (\bar{H}_i^{v*} + \bar{H}_i^{I*}) : \bar{E}^*(\vec{r}_i)\right)$$

$$+ \vec{Y}_{i+1}^* - \vec{Y}_i^*) \times \hat{z}_i,$$

where $\bar{\bar{C}}_{z_i}^*$ is a second-order tensor and is a function of the tensor $\left(\dot{\bar{I}}_i^* + \frac{1}{\Delta t^*} \bar{I}_i^* + \bar{\bar{C}}_i^{v^*} + \bar{\bar{C}}_i^{I^*} \right)^{-1}$ and the orientation vector \hat{z}_i . After applying Tikhonov regularization (see Andrić (2012)), this system can be solved for the unknown dimensionless connectivity forces $\bar{X}_{i,n}^*$, $2 \leq i \leq N$, with $\bar{X}_{1,n}^* = \bar{X}_{N+1,n}^* = 0$. After computing the dimensionless velocities and scaling them back to their dimensional form, new segment positions and orientations can be computed as

$$\vec{r}_{i,n} = \vec{r}_{i,n-1} + \Delta t \dot{\vec{r}}_{i,n} \quad (27)$$

$$\hat{z}_{i,n} = \hat{z}_{i,n-1} + \Delta t (\bar{\omega}_{i,n} \times \hat{z}_{i,n-1}). \quad (28)$$

A correction of the segment positions is done at each time step to preclude the accumulation of errors. As in the algorithm implemented by Lindström and Uesaka (2007), the middle fiber segment is fixed in space and all the other segments are translated to maintain the exact original fiber length.

Numerical Stability and Time Step Constraints. Assuming the worst case from the point of stability—that the inertia terms are zero—and using expressions (9) and (11), the hydrodynamic force on segment i , flowing in a stationary fluid, can be estimated as

$$|\bar{F}_i^h| \sim \eta d \Delta v, \quad (29)$$

so that

$$m_i |\ddot{\vec{r}}_i| \sim \eta l |\dot{\vec{r}}_i|. \quad (30)$$

Denoting the speed of the segment by v , Eq. (30) is essentially a first-order, ordinary differential equation, which can be written in the form

$$\dot{v} + C_1 v \sim 0, \quad (31)$$

where $C_1 = \frac{\eta l}{m_i}$. The stability condition for this type of equation imposes the time step constraint

$$\Delta t \ll \frac{1}{C_1} = \frac{m_i}{\eta l}. \quad (32)$$

From Eq. (20), the bending torque for fiber segment i can be estimated as $|\vec{Y}_i^b| \sim E_Y I_i \Delta \theta_i / l_i$, where

$\Delta \theta_i = \arccos(\hat{z}_i \cdot \hat{z}_i^{eq})$ is the deviation angle from the equilibrium shape. From expressions (10) and (12), the hydrodynamic torque on segment i is estimated as $|\bar{T}_i^h| \sim \eta l_i^3 |\bar{\omega}_i|$, when inertia terms are neglected. The magnitude of the hydrodynamic torque $|\bar{T}_i^h|$ must be comparable to the magnitude of the bending torque $|\vec{Y}_i^b|$, i.e.

$$\eta l_i^3 |\bar{\omega}_i| \sim \frac{E_Y I_i \Delta \theta_i}{l_i}, \quad (33)$$

which yields

$$|\bar{\omega}_i| \sim \frac{E_Y I_i}{\eta l_i^4} \Delta \theta_i. \quad (34)$$

Since $|\bar{\omega}_i| = d(\Delta \theta_i)/dt$, Eq.(34) also represents a first-order differential equation

$$d(\Delta \theta_i)/dt + C_2 \Delta \theta_i \approx 0 \quad (35)$$

and $C_2 = E_Y I_i / \eta l_i^4$. The time step constraint is again given as

$$\Delta t \ll \frac{1}{C_2} = \frac{\eta l_i^4}{E_Y I_i}.$$

Results and Validation

In this section, the results of the numerical simulations using the implemented model are compared to three different experiments available in the literature. The implementation of the fiber inertia was validated by Andrić (2012) for the period of a two-segment physical pendulum. The simulated period was in excellent agreement with the analytical solution.

Individual Fiber Motion in Shear Flow. Jeffery (1922) studied the motion of isolated prolate spheroids in simple shear flow. He showed that a prolate spheroid with an aspect ratio r_s undergoes periodic motion, so-called Jeffery orbits, and it spends most of the time aligned with the flow direction. The period of revolution is $T = 2\pi(r_s + 1/r_s)/\dot{\gamma}$ and increases with r_s . This relation can use an effective aspect ratio for non-spheroidal particles. Bretherton (1962) showed that any axisymmetric particle in a linear flow gradient rotates with a period $T = 2\pi(r_e + 1/r_e)/\dot{\gamma}$, where r_e is an equivalent aspect ratio that depends on the particle shape. The equivalent aspect ratio for a circular cylinder is given by Eq. (7). Forgacs and Mason (1959a) theoretically studied the deformation of cylindrical particles rotating in shear flow. They derived the equations to calculate the critical value of $\dot{\gamma}\eta$ at which the axial compression due to shear will cause

the fiber to buckle. Schmid et al. (2000) used the dimensionless group, named bending ratio (BR), to predict the bending of a cylindrical fiber in the flow-gradient plane, where

$$\text{BR} \equiv \frac{E_Y (\ln(2r_e) - 1.50)}{(\eta\dot{\gamma})2r_f^4} \quad (37)$$

with $r_f = L_f/d$, where L_f is the fiber length and d is its diameter.

Regimes of Fiber Motion in Shear Flow. Forgacs and Mason (1959b) experimentally studied the orbiting behavior of flexible fibers in shear flow, varying fiber length, fiber stiffness, shear rate and fluid viscosity. In this work, we chose three experimental instances, which correspond to rigid, springy and snake-like regime, respectively, to make qualitative comparison with the numerical simulations. The geometrical characteristics of the fibers and the flow parameters are summarized in Table 1.

L_f [mm]	d [μm]	r_f [-]	$\dot{\gamma}\eta$ [Pas]	Orbit type
1.40	7.8	180	469	Rigid
2.42	7.8	310	445	Springy
3.23	7.8	414	440	Snake-like

Table 1: The parameter settings for three experimental samples described by Forgacs and Mason (1959b) and numerically studied by Lindström and Uesaka (2007). The fiber material is Dacron with Young's modulus $E_Y = 2\text{GPa}$.

Comparison with Experiments. We carried out the simulations of an isolated fibers in simple shear flow using the implemented model. The computational domain is a box of side 0.01 m and it is discretized into a rectangular mesh with ten cells in each direction. The number of cells is chosen to make sure that interpolation of the prescribed flow field at the segment centers is taking place in non-boundary cells only, preserving a second-order interpolation of the linear velocity distribution. The time series of images from the separate simulations for the corresponding orbit types are shown in Fig. 2. The fibers are initially aligned with the flow. In the case of a rigid orbit, the equilibrium shape of the fiber is straight. For springy and snake-like orbits the equilibrium fiber shape is a U-shape with an intrinsic radius of curvature $R_u = 100L_f$, to mimic the geometrical imperfection of the physical fibers. The evolution of the fiber shapes reproduce those observed by Forgacs and Mason (1959b). We compare the simulated orbit period of the rigid fiber with the one computed using Jeffery's equation in conjunction with Cox's equation for the equivalent aspect ratio of a circular cylinder. The simulated orbiting period is overestimated by 20%. This discrepancy is due to the one-way coupling between the fiber and the fluid phase (Lindström and Uesaka 2007). For the rigid, springy and snakelike regime, we find that the simulated orbits are

in qualitative agreement with the experimental observations for each orbit type.

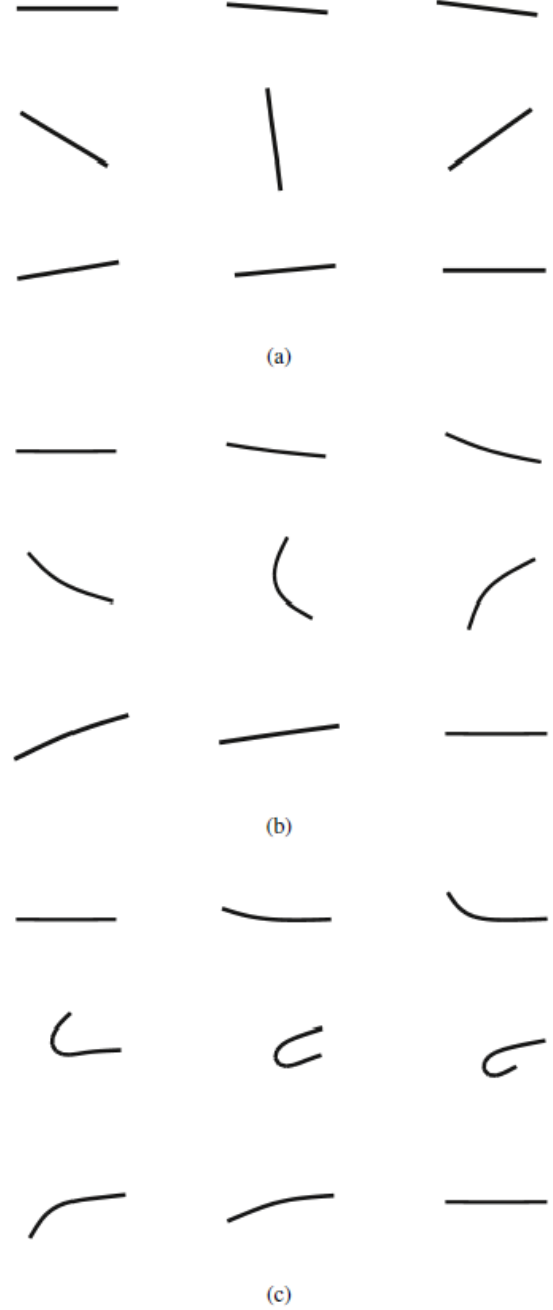


Figure 2: The time series of images show the simulation results for the fiber shape development in a simple shear flow for half of a period of revolution. Each case corresponds to an actual experiment by Forgacs and Mason (1959b). Three different orbit types a)rigid, b)springy, and c)snake-like are observed. The fiber diameters are exaggerated for the purpose of visualization.

Conclusions

A particle-level fiber model has been integrated into a

general-purpose CFD code. The fibers are modeled as chains of cylindrical segments and their motion is described by Euler's first and second law for each segment. All the degrees of freedom necessary to realistically reproduce the dynamics of real fibers, are taken into account. The implemented model was validated against known analytical and experimental results for fiber motion in shear flow. It was found that the model reproduces the known orbiting behavior for rigid and flexible fibers in low segment Reynolds number shear flow.

Acknowledgements

The financial support from Bo Rydin Foundation and SCA Hygiene Products AB is gratefully acknowledged.

References

- J. Andrić. Implementation of a flexible fiber model in a general-purpose CFD code. Thesis for Licentiate of Engineering no. 2012:04, Chalmers University of Technology, Göteborg, Sweden, 2012.
- F.P. Bretherton. The motion of rigid particles in a shear flow at low Reynolds number, *J. Fluid Mech.* 14, 284–304, 1962.
- R. G. Cox. The motion of long slender bodies in a viscous fluid. Part 2. Shear flow. *J. Fluid Mech.*, 45:625–657, 1971
- C. T. Crowe, M. Sommerfeld, and Y. Tsuji. *Multiphase Flows With Droplets and Particles*. CRC, New York, 1998.
- O. L. Forgacs and S. G. Mason. Particle motions in sheared suspensions. IX. Spin and deformation of threadlike particles. *J. Colloid Sci.*, 14:457–472, 1959a.
- O. L. Forgacs and S. G. Mason. Particle motions in sheared suspensions. X. Orbits of flexible threadlike particles. *J. Colloid Sci.*, 14:473–491, 1959b.
- J. Hämäläinen, S. B. Lindström, T. Hämäläinen, and T. Niskanen. Papermaking fiber suspension flow simulations at multiple scales. *J. Eng. Math.*, 71(1):55–79, 2011.
- G. B. Jeffery. The motion of ellipsoidal particles immersed in a viscous fluid. *Proc. Roy. Soc. London Ser. A*, 102:161–179, 1922.
- S. Kim and S.J. Karilla. *Microhydrodynamics: Principles and Selected Applications*. Butterworth–Heinemann, Stoneham, 1991.
- S. B. Lindström. Modeling and simulation of paper structure development. PhD thesis, Mid Sweden University, Sundsvall, Sweden, October 2008.
- T. Matsuoka and S. Yamamoto. Dynamic simulation of fiber suspensions in shear flow. *J. Chem. Phys.*, 102:2254–2260, 1995.
- D. Qi. Direct simulations of flexible cylindrical fiber suspensions in finite Reynolds number flows. *J. Chem. Phys.*, 125:114901, 2006.
- R. F. Ross and D. J. Klingenberg. Dynamic simulation of flexible fibers composed of linked rigid bodies. *J. Chem. Phys.*, 106:2949–2960, 1997.
- A. Salahuddin, J.Wu, and C. K. Aidun. Numerical study of rotational diffusion in sheared semidilute fiber suspension. *J. Fluid Mech.*, 692:153–182, 2012.
- C. F. Schmid, L. H. Switzer, and D. J. Klingenberg. Simulation of fiber flocculation: Effects of fiber properties and interfiber friction. *J. Rheol.*, 44:781–809, 2000.
- E.Svenning, A. Mark, F. Edelvik, E. Glatt, S. Rief, A. Wiegmann, L. Martinsson, R. Lai, M. Fredlund, and U. Nyman. Multiphase simulation of fiber suspension flows using immersed boundary methods. *Nordic Pulp Paper Res. J.*, 27(2):184–191, 2012.
- D. J. Tritton. *Physical fluid dynamics*. Clarendon, Oxford, 1988.
- H.G. Weller, G. Tabor, H. Jasak, and C.Fureby. A tensorial approach to computational continuum mechanics using object-oriented techniques. *Comput. Phys.*, 12(6): 620–631, 1998.